Int. J. Multiphase Flow Vol. 11, No. 4, pp. 515–533, 1985
Printed in the U.S.A.

0301-9322/85 $3.00 + .00

A TWO-EQUATION TURBULENCE MODEL FOR JET FLOWS LADEN WITH VAPORIZING DROPLETS

A. A. MOSTAFA and S. E. ELGHOBASHI
Mechanical Engineering Department, University of California, Irvine, CA 92717, U.S.A.

(*Received* 5 *May* 1984; *in revised form* 23 *August* 1984)

Abstract—A two-equation turbulence model for steady incompressible two-phase flows including phase change has been recently developed by Mostafa & Elghobashi (1984). This model is tested for the flow of a turbulent axisymmetric gaseous jet laden with evaporating liquid droplets. To avoid the problem of density fluctuations of the carrier phase at this stage, only isothermal flow is considered and vaporization is assumed to be due to the vapor concentration gradient. The continuous size distribution of the droplets is approximated by finite size groups. Each group is considered as a continuous phase interpenetrating and interacting with the carrier phase. Two test cases have been predicted by the model. The first is for a Freon-11 spray issuing from a round nozzle, where experimental data are available at distances equal to or greater than 170 nozzle diameters. Good agreement between the data and the predictions was achieved. The second is for a methanol spray where no experiments are available yet, and the predictions consider the flow region close to the nozzle ($z/D < 40$). The results of the methanol spray include distributions of the mean velocity, volume fractions of the different phases, concentration of the evaporated material in the carrier phase, turbulence intensity and shear stress of the carrier phase, droplet diameter distribution, and the jet spreading rate. In this case the results are analyzed based on a qualitative comparison with the corresponding single phase jet flow.

1. INTRODUCTION

Accurate prediction of spray combustion is extremely difficult due to the complex physical and chemical phenomena encountered in this two-phase process. The interaction between droplets and the turbulent fluid, turbulence effects on chemical reaction and heat transfer (and hence on droplet vaporization) are just a few examples of the complexity. In order to understand the nature of these interactions, coordinated experimental and theoretical studies need to be performed in a stepwise manner thus isolating the phenomenon to be investigated. A turbulent nonreacting gaseous jet laden with evaporating droplets is a relatively simple flow which allows the study of the interactions between the two phases, the turbulent dispersion of the liquid droplets, and the droplet size distribution. Also, the turbulent round jet laden with evaporating liquid droplets is important in its own right. Premixed–prevaporized gas turbine combustor, diesel-engine sprays, spray-cooling and spray-drying systems, and rocket plumes are some examples of this type of flow.

Existing data on the mean and turbulent structure of evaporating sprays are restricted to the region far downstream from the nozzle and so far do not provide adequate support for mathematical modeling work. Yule *et al.* (1982) reported measurements in evaporating sprays from a twin-fluid injector in a coflowing stream, but they did not report the radial profiles of the main dependent variables throughout the flow field. This information is essential for accurately predicting such flow. Wu *et al.* (1984) measured the mean and the turbulence quantities of dense fuel spray in a round gaseous jet. These measurements cover the region far downstream ($300 \leq z/D \leq 800$) from the nozzle and thus information about the jet development region is not available. Also they did not measure all the radial profiles needed for the input to the numerical solution.

There have been, however, several attempts to predict the behavior of particle-laden jets. Mostafa & Elghobashi (1984) discussed those attempts and indicated that the available models ignore many significant correlations created by the presence of the dispersed phase in the same control volume of the carrier phase. Shuen *et al.* (1983) evaluated the performance of the existing dispersion models by comparing the predictions with existing measurements

of particle-laden jets. They indicated that their stochastic separated flow model in contrast to the other models provides reasonably good predictions over the data base. In their work the conventional k-ϵ model for single-phase flows was used without any modifications. In fact ignoring the turbulence correlations created by the presence of the dispersed phase led to the failure of many previous attempts as discussed by Mostafa & Elghobashi (1984).

Elghobashi & Abou-Arab (1983) proposed a two-equation turbulence model for incompressible dilute two-phase flows which undergo no phase changes. Using this model, Elghobashi *et al.* (1984) predicted the turbulent axisymmetric gaseous jet laden with uniform size solid particles. They achieved good agreement with the experimental data of Modarress *et al.* (1984). This model has been extended by Mostafa & Elghobashi (1984) to include the effects of phase changes

Shearer *et al.* (1979) measured the mean velocity, velocity fluctuations and Reynolds stress of single-phase constant density jets, as well as those of an evaporating spray (Freon-11 with a Sauter mean diameter equal to 29 μ) in the region far downstream from the nozzle ($170 \leq z/D \leq 510$). In this region we will compare the predictions with Shearer's *et al.* (1979) data. In the jet-developing region (very close to the nozzle) the model is applied to predict the turbulent round jet laden with multisize evaporating methanol droplets. The distributions of the mean velocities, volume fractions of the carrier phase and the liquid droplets, turbulence intensity, shear stress of the carrier phase, the droplet diameter distribution and the jet spreading rate are presented. The droplet material is chosen as methanol since the density of the methanol vapor nearly equals that of atmospheric air. Thus we can avoid the complications of the density fluctuations of the carrier phase.

2. *Mathematical model*

This section describes the assumptions and the forms of the modeled transport equations with appropriate boundary conditions for predicting turbulent gaseous jet flows laden with vaporizing droplets.

It is assumed that no droplet coalescensce or breakup occurs. This implies that the droplets are sufficiently dispersed so that droplet collisions are infrequent. The initial breakup of liquid sprays or jets is not considered. It is assumed that the initial profiles of volume fractions and velocities are independently specified. The droplets are considered as a continuous phase interpenetrating and interacting with the gas phase. The droplets are classified into finite size groups. Further we assume constant properties for both the carrier fluid and droplets.

This leads to two sets of transport equations, one set for the droplets and the other for carrier phase (primary air issuing from the pipe plus the evaporated material). These equations will be coupled primarily by three mechanisms, the mass exchange, the displacement of the carrier phase by the volume occupied by droplets and momentum interchange between droplets and the carrier phase. The momentum interchange is due to the aerodynamic forces exerted on the dispersed phase and the momentum growth resulting from the relative velocity between the generated vapor and the surrounding gas. The turbulent characteristics of the carrier phase are described by a two-equation turbulence model based on the rigorously derived equations for the turbulence kinetic energy and its dissipation rate. All the governing equations to predict the mean and turbulence quantities for turbulent two-phase flows including phase changes, the assumptions for this study and the solution methodology were discussed in detail by Mostafa (1985); they will be cast here in the modeled form in cylindrical coordinates for the axi-symmetric jet flow.

2.1 *Governing equations*

Droplets equation. The momentum equation for droplets having an average diameter d^k in the kth diameter range in the axial (z) direction is given by Mostafa & Elghobashi

(1984),

$$\begin{aligned}\rho_2\Phi^k V_z^k V_{z,z}^k + \rho_2\Phi^k V_r^k V_{z,r}^k = &-\Phi^k P_{,z} + F^k\Phi^k(U_z - V_z^k) \\ &+ \frac{1}{r}(\Phi^k r\rho_2\nu_p^k V_{z,r}^k)_{,r} + c_{m1}\rho_2 V_{z,r}^k\left(\frac{\nu_p^k}{\sigma_\phi}\Phi_{,r}^k\right) \\ &+ c_{\phi 5}\rho_2\frac{1}{r}\left(\frac{k}{\epsilon}r\nu_p^k V_{z,r}^k\right)_{,r}\left(\frac{\nu_P^k}{\sigma_\phi}\Phi_{,r}^k\right)_{,r} \\ &+ c_{\phi 5}\frac{k}{\epsilon}\mu_p^k V_{z,r}^k\left(\frac{\nu_P^k}{\sigma_\phi}\Phi_{,r}^k\right)_{,rr} + (\rho_2 - \rho_1)g\Phi_k.\end{aligned} \tag{1}$$

The mean continuity equation of the kth group is

$$\rho_2(\Phi^k V_z^k)_{,z} + \rho_2(\Phi^k V_r^k)_{,r} - \rho_2\left(\frac{\nu_P^k}{\sigma_\phi}\Phi_{,z}^k\right)_{,z} - \frac{\rho_2}{r}\left(r\frac{\nu_P^k}{\sigma_\phi}\Phi_{,r}^k\right)_{,r} = -\dot{m}^k\Phi^k. \tag{2}$$

Carrier phase equations. The momentum equation for the carrier phase in the axial (z) direction is given by

$$\begin{aligned}\rho_1\Phi_1 U_z U_{z,z} + \rho_1\Phi_1 U_r U_{z,r} = &-\Phi_1 P_{,z} - \sum_k \Phi^k(F^k + \dot{m}^k)(U_z - V_z^k) \\ &+ \frac{1}{r}(\Phi_1\rho_1 r\nu_t U_{z,r})_{,r} + c_{m1}\rho_1 U_{z,r}\left(\frac{\nu_t}{\sigma_\phi}\Phi_{1,r}\right) \\ &+ c_{\phi 5}\rho_1\frac{1}{r}\left(\frac{k}{\epsilon}r\nu_t U_{z,r}\right)_{,r}\left(\frac{\nu_t}{\sigma_\phi}\Phi_{1,r}\right)_{,r} \\ &+ c_{\phi 5}\frac{k}{\epsilon}\mu_t U_{z,r}\left(\frac{\nu_t}{\sigma_\phi}\Phi_{1,r}\right)_{,rr}.\end{aligned} \tag{3}$$

The mean global continuity is

$$\Phi_1 + \sum_k \Phi^k = 1, \tag{4}$$

where $c_{m1} = 0.4$ and $c_{\phi 5} = 0.1$.

In the above equation the comma-suffix notation indicates differentiation with respect to the spatial coordinates z and r. U and V^k are, respectively, the mean velocity of the carrier fluid and the droplets in the kth diameter range. The superscript k denotes the kth group of the dispersed phase. The subscripts 1 and 2 denote, respectively, the carrier fluid and the dispersed phase. ρ is the material density. ν_t and ν_p are the kinematic eddy viscosity of the carrier phase and its corresponding value for the droplets, respectively. P is the mean pressure, Φ is the volume fraction, g is the gravitational acceleration, F is the interphase friction coefficient and $\dot{m}$ is the mass evaporated per unit time and unit droplet volume.

The momentum equations of both phases in the radial direction can be written in a similar manner and will not be presented here.

The quantities F^k, $\dot{m}^k$ and ν_p^k are evaluated in the following section.

The interphase friction factor F^k. In the governing equations set, the drag force is expressed in terms of the interphase friction coefficient F^k. In general, F^k is given by

$$F^k = (3/4d^k)\,\rho_1 C_D^k\,|\,\mathbf{U} - \mathbf{V}^k\,|\,. \tag{5}$$

The drag coefficient C_D^k is primarily a function of the Reynolds number based on the total relative velocity but may also depend on the evaporation rate.

Droplet evaporation tends to reduce the friction drag coefficient only at very high evaporation rates (such as for droplets burning in pure oxidizing atmosphere), therefore the effect of mass transfer on the drag coefficient will be neglected.

The internal circulation of the liquid droplet decreases the boundary layer thickness of the exterior flow and may reduce the drag coefficient. But the effect is again very small.

Ingebo (1956) investigated the drag coefficients for liquid droplets and solid spheres accelerating in air streams using a high-speed camera technique. Sphere diameters range was 20 to 120 μ. To ensure the spherical shape for the liquid droplets (isooctane, water and trichloroethylene), the Reynolds number was in the range $6 < \mathrm{Re}^k < 400$. The main purpose of Ingebo's work was the study of the effects of the rate of acceleration, and the evaporation rate on the drag coefficient. His main conclusion is that the unsteady-state drag coefficients are different from the steady-state values but when the acceleration rates are low, the unsteady-state drag coefficients are in agreement with the steady state values of previous investigations. In addition, Ingebo concluded that the drag coefficient for slowly evaporating droplets, nonevaporating droplets and solid spheres are the same. This means that for evaporating droplets there is a balance between the decrease in friction drag due to the internal circulation and the increase in pressure drag due to the blowing effects associated with vaporization (Sirignano 1983). Thus the droplet drag coefficient is almost the same as that for a solid sphere of the same diameter. In the present case (low evaporation rate of a spherical liquid droplet in gas) the drag coefficient can be prescribed according to the standard experimental drag curve of a sphere in a steady motion. Clift *et al.* (1978) represented this curve by:

$$C_D^k = \frac{24}{\mathrm{Re}^k}\left(1 + 0.135\,(\mathrm{Re}^k)^{0.82-0.05w}\right), \qquad 0.01 < \mathrm{Re}^k \leq 20; \qquad [6]$$

$$C_D^k = \frac{24}{\mathrm{Re}^k}\left(1 + 0.1935\,(\mathrm{Re}^k)^{0.6305}\right), \qquad 20 < \mathrm{Re}^k \leq 200; \qquad [7]$$

where $w = \mathrm{Log}_{10}\mathrm{Re}^k$ and the droplet Reynolds number is calculated from

$$\mathrm{Re}^k = |\,\mathbf{U} - \mathbf{V}^k\,|\, d^k/\nu_1. \qquad [8]$$

where ν_1 is the kinematic viscosity of the carrier phase.

Mass transfer rate $\dot{m}^k$. The evaporation rate or the time rate of change of droplet diameter is determined by the kind of physicochemical evaporative process and the nature of the surrounding flow. If changes in the droplet size and flow conditions occur sufficiently slowly, the time derivatives in the differential equations governing the evaporation rate may be neglected and the quasi-steady-state evaporation relation applies.

For the quasi-steady-state evaporation of a spherical droplet suspended in a moving stream the mass evaporated per unit time and unit droplet volume is given by

$$\dot{m}^k = \frac{12\delta\rho_1}{(d^k)^2}\ln(1 + B)\mathrm{Sh}^k, \qquad [9]$$

where δ is the molecular diffusivity of evaporated material in air, B is the transfer number and Sh^k is the Sherwood number given by [14].

Here, evaporation occurs due to the concentration gradient; the transfer number is given by

$$B = (C_L - C)/(1 - C_L), \qquad [10]$$

where C, C_L are the concentrations (defined as the ratio of the mass of the evaporated material within a control volume to the mass of the carrier phase in the same volume) of the evaporating material at the free stream conditions and the droplet surface respectively. C is obtained from the solution of the modeled concentration transport equation:

$$\rho_1\Phi_1U_zC_{,z} + \rho_1\Phi_1U_rC_{,r} = \frac{1}{r}\left(\rho_1 r\Phi_1\frac{\nu_t}{\sigma_c}C_{,r}\right)_{,r} + \sum_k \Phi^k\dot{m}^k(1 - C) + \rho_1 C_{,r}\left(\frac{\nu_t}{\sigma_\phi}\Phi_{1,r}\right), \quad [11]$$

where σ_c is a constant of value 0.7.

C_L is obtained from Clausius–Clapeyron expression; which reads

$$C_L = \frac{X_v W_v}{X_v W_v + (1 - X_v)W_a}, \quad [12]$$

where

$$X_v = \frac{P_o}{P}\exp\left(\frac{W_v L}{R_o}\left(\frac{1}{T_B} - \frac{1}{T_L}\right)\right), \quad [13]$$

P_o and P are the atmospheric pressures and the partial pressures of the evaporating material at the droplet surface, respectively. W_v and X_v are the molecular weight and the molecular fraction of the evaporating material, respectively; T_B and T_L are the boiling and saturation temperatures of the evaporating material and R_0 is the universal gas constant. L is the latent heat of vaporization/unit mass.

The Sherwood number in [9] is given by the semiempirical formula of Ranz & Marshall (1952) as

$$\mathrm{Sh}^k = \frac{\dot{m}^k}{\pi d^k\delta(C_L - C)} = 2 + 0.55\,\mathrm{Re}^{k^{1/2}}\mathrm{Sc}^{1/3}, \quad [14]$$

where $\mathrm{Sc} = \nu_1/\delta$ is the Schmidt number.

Although in the present work evaporation occurs due to the concentration gradient only, effects of temperature gradients can be included in a straightforward manner. This stepwise approach is adopted to avoid the complications of the density fluctuation of the carrier phase due to temperature differences between the liquid droplets and the surrounding gas.

Turbulent diffusivity of liquid droplets ν_p^k. The turbulent diffusivity of liquid droplets (ν_p^k) is evaluated by introducing the droplet Schmidt number σ_p^k defined as

$$\sigma_p^k = \frac{\nu_t}{\nu_p^k}, \quad [15]$$

where ν_t is the turbulent diffusivity of the carrier phase [$\nu_t = c_\mu(k^2/\epsilon)$] where the value of c_μ is given in table 2. Since the liquid droplets do not in general follow the motion of the surrounding fluid from one point to another it is expected that σ_p^k will be different from unity and vary with the particle relaxation time and local turbulence quantities. Alonso (1981) reviewed the recent developments in evaluating σ_p^k and recommended the use of Peskin's (1971) formula

$$\nu_p^k/\nu_t = (1/\sigma_p^k) = 1 - (3/2)\,L_R^2\,[Q^2/(Q + 2)], \quad [16]$$

where

$$Q = (2\rho_2/F^kT_L). \quad [17]$$

Table 1. Experimental flow conditions at 170 D downstream of the injection nozzle (Shearer *et al.* 1979)

	U, m/s		k, m^2/s^2		$\epsilon \times 10^{-2}$ m^2/s^3			
r, mm	S.ph.	Spray	S.ph.	Spray	S.ph.	Spray	$\Phi_2 \times 10^6$ m^3 droplet/m^3	C kg vapor/kg
0.0	9.6	11.7	7.1	9.6	7.06	17.4	2.25	0.24
5.0	9.0	11.0	7.1	9.6	7.06	17.4	1.8	0.22
10.0	7.9	9.41	6.8	9.3	5.42	15.2	1.2	0.19
15.0	6.2	7.30	6.0	8.7	3.35	5.98	0.51	0.14
20.0	3.6	5.20	4.5	7.2	2.04	6.29	0.2	0.09
25.0	3.2	3.27	3.0	5.2	1.17	3.92	0.14	0.05
30.0	2.1	1.93	1.8	3.1	0.487	1.56	0.08	0.02
35.0	1.1	0.94	0.09	1.4	0.25	0.53	0.04	0.01
40.0	0.4	0.0	0.03	0.0	0.1	0.0	0.0	0.0
42.5	0.0		0.0		0.0			

L_R is a length scale ratio L_L/λ. The local Lagrangian integral time scale T_L is given by Calabrese & Middleman (1979) as

$$T_L = (5/12)k/\epsilon. \qquad [18]$$

The local Lagrangian length scale L_L and the Eulerian microscale λ are given by

$$L_L = \sqrt{\frac{2}{3}k}\,T_L, \qquad [19]$$

$$\lambda = \sqrt{10\,\nu_1 k/\epsilon}. \qquad [20]$$

Soo (1967) indicated that the Peskin's formula only represents an approximation because of the neglect of higher-order terms in the derivation. Soo obtained good agreement between this formula and his experimental data by setting λ equal to half of the duct diameter. Hinze (1975) argued that the calculated Schmidt number using Peskin's formula is around unity due to the limitations inherent in Peskin's assumptions and solution. Using Peskin's formula in the present work resulted in a negative Schmidt number in most of the flow domain. Numerical study was performed to optimize the length scale ratio to produce agreement with experiment (Elghobashi *et al.* 1984). This length scale ratio is given by

$$L_R = l/R, \qquad [21]$$

where R is the local jet width, and l is the dissipation length scale, calculated from

$$l = C_\mu^{3/4}\,k^{3/2}/\epsilon. \qquad [22]$$

The turbulence model. The modeled form of the turbulence kinetic equation (k) of the carrier fluid; according to Mostafa & Elghobashi (1984) is

$$\begin{aligned}
&\rho_1\Phi_1 U_z k_{,z} + \rho_1\Phi_1 U_r k_{,r} = \rho_1\Phi_1\nu_t U_{z,r}U_{z,r} - \frac{4}{3}\rho_1 c_{\phi 5}\left(\frac{\nu_t}{c_\mu}\right)\left(\frac{\nu_t}{\sigma_\phi}\Phi_{1,r}\right)_{,r} U_{r,r} \\
&+ \rho_1 c_{\phi 5}\left(\frac{k}{\epsilon}\right)\nu_t\left(\frac{\nu_t}{\sigma_\phi}\Phi_{1,r}\right)_{,r} U_{z,r}U_{z,r} - \sum_k k\Phi^k(F^k + \dot{m}^k)\left(1 - \int_0^\infty\left(\frac{\Omega_1 - \Omega_R}{\Omega_2}\right)F(\omega)\,\mathrm{d}\omega\right) \\
&+ \sum_k (F^k + \dot{m}^k)\left[(U_r - V_r^k)\left(\frac{\nu_p^k}{\sigma_\phi}\Phi_{,r}^k\right) - c_{\phi 5}\left(\frac{\nu_t}{c_\mu}\right)\left(\frac{\nu_p^k}{\sigma_\phi}\Phi_{,r}^k\right)_{,r}\left(1 - \int_0^\infty\left(\frac{\Omega_1 - \Omega_R}{\Omega_2}\right)F(\omega)\,\mathrm{d}\omega\right)\right] \\
&+ \frac{1}{r}\left(\rho_1\Phi_1\frac{\nu_t}{\sigma_k}rk_{,r}\right)_{,r} - \rho_1\Phi_1\epsilon.
\end{aligned} \qquad [23]$$

The turbulence energy dissipation rate (ϵ) is

$$\begin{aligned}
&\rho_1\Phi_1 U_z\epsilon_{,z} + \rho_1\Phi_1 U_r\epsilon_{,r} = c_{\epsilon 1}\frac{\epsilon}{k}\rho_1\Phi_1\left[\nu_t U_{z,r}U_{z,r}\right. \\
&\left. - \frac{4}{3}\frac{c_{\phi 5}}{\Phi_1}\left(\frac{\nu_t}{c_\mu}\right)\left(\frac{\nu_t}{\sigma_\phi}\Phi_{1,r}\right)_{,r} U_{r,r} + \frac{c_{\phi 5}}{\Phi_1}\left(\frac{k}{\epsilon}\right)\nu_t\left(\frac{\nu_t}{\sigma_\phi}\Phi_{1,r}\right)_{,r} U_{z,r}U_{z,r}\right] \\
&-c_{\epsilon 3}\frac{\epsilon}{k}\left[\sum_k (F^k + \dot{m}^k)\left(\Phi^k k\left(1 - \int_0^\infty\left(\frac{\Omega_1 - \Omega_R}{\Omega_2}\right)F(\omega)\mathrm{d}\omega\right)\right.\right. \\
&\left.\left. - (U_r - V_r^k)\left(\frac{\nu_p^k}{\sigma_\phi}\Phi_{,r}^k\right) + c_{\phi 5}\left(\frac{\nu_t}{c_\mu}\right)\left(\frac{\nu_p^k}{\sigma_\phi}\Phi_{,r}^k\right)_{,r}\left(1 - \int_0^\infty\left(\frac{\Omega_1 - \Omega_R}{\Omega_2}\right)F(\omega)\mathrm{d}\omega\right)\right)\right] \\
&+ \frac{1}{r}\left(\rho_1 r\Phi_1\frac{\nu_t}{\sigma_\epsilon}\epsilon_{,r}\right)_{,r} - c_{\epsilon 2}\rho_1\Phi_1\frac{\epsilon^2}{k}.
\end{aligned} \tag{24}$$

The terms in [23] and [24], involving integration in the frequency domain (ω) represent additional dissipation of k or ϵ due to the slip between the droplets and the carrier fluid and depend on the magnitude of correlation between their respective instantaneous velocities. Details of the derivation of these terms are given by Elghobashi & Abou-Arab (1984).

The Lagrangian frequency function $F(\omega)$ is in general affected by the presence of the dispersed phase. In the low frequency range (inertial subrange), the modulation of the Lagrangian frequency function of the carrier fluid by the dispersed phase can be neglected (Altaweel & Landau 1977). Thus in the present work the Lagrangian frequency function is given by Hinze (1975).

$$F(\omega) = \left(\frac{2}{\pi}\right)\left(\frac{T_L}{1 + \omega^2 T_L^2}\right), \tag{25}$$

where ω ranges from 1 to 10^4 (s^{-1}) and T_L is calculated from [18]. The functions Ω_1, Ω_2, Ω_R, α and β are evaluated according to Chao (1964):

$$\begin{aligned}
\Omega_1 &= \left(\frac{\omega}{\alpha}\right)^2 + \sqrt{6}\left(\frac{\omega}{\alpha}\right)^{3/2} + 3\left(\frac{\omega}{\alpha}\right) + \sqrt{6}\left(\frac{\omega}{\alpha}\right)^{1/2} + 1; \\
\Omega_2 &= \beta^{-2}\left(\frac{\omega}{\alpha}\right)^2 + \sqrt{6}\,\beta^{-1}\left(\frac{\omega}{\alpha}\right)^{3/2} + 3\left(\frac{\omega}{\alpha}\right) + \sqrt{6}\left(\frac{\omega}{\alpha}\right)^{1/2} + 1; \\
\Omega_R &= [(1 - \beta)\omega/(\alpha\beta)]^2; \\
\alpha &= C_D^k|\,\mathbf{U} - \mathbf{V}^k\,|/2d^k; \\
\beta &= 3\rho_1/(2\rho_2 + \rho_1).
\end{aligned} \tag{26}$$

The values of the coefficients appearing in [23] and [24] are listed in Table 2 below.

Table 2. Coefficients of the turbulence model

σ_ϕ	σ_k	c_μ	σ_ϵ	$c_{\phi 5}$	$c_{\epsilon 1}$	$c_{\epsilon 2}$	$c_{\epsilon 3}$
1	1	$k - \epsilon$[1]	1.3	0.1	1.44	$k - \epsilon$[1]	1.2

[1]See Launder, Morse, Rodi and Spalding (1972).

It is seen that three new coefficients (σ_ϕ, $c_{\phi 5}$, $c_{\epsilon 3}$) are now added to the well-established k-ϵ coefficients for single-phase flows, namely σ_k, σ_ϵ, c_μ, $c_{\epsilon 1}$ and $c_{\epsilon 2}$. The values of the new coefficients have been optimized by Elghobashi *et al.* (1984).

3. NUMERICAL SOLUTION PROCEDURE

The marching finite-difference solution procedure employed in this work is that developed and described in detail by Spalding (1979). Also the modifications for the phase change, the turbulence effects and the multisize consideration are described in Mostafa & Elghobashi (1984).

4. THE FLOWS CONSIDERED

The only available experimental data for an evaporating spray are those of Shearer *et al.* (1979). However, these measurements provide information about the flow only far downstream from the injection nozzle ($z/D \geq 170$). This represents the first flow to test our model. The second flow is that of a methanol spray for which no experimental data exist and we predict the flow region close to the nozzle ($0.1 \leq z/D \leq 40$). The predictions of this flow are compared qualitatively with those of a single phase jet to examine the effects of vaporization on the flow.

4.1 *The flow of shearer et al. (Freon-11 Spray)*

Shearer *et al.* (1979) measured the carrier phase properties using laser doppler anemometer, the droplet size distribution and the liquid mass flux using inertial impaction method in a turbulent round jet. The Freon-11 spray was generated by an air-atomizing nozzle of 1.194 mm outer diameter (D). The ratio of the mass flow rate of Freon-11 droplets at the nozzle exit to that of the air (X_0) is equal to 6.88 and the initial average velocity, $U_{z,0}$ = 74.45 m/s. They also measured the mean mixture fraction by isokinetically sampling the flow at the gas velocity.

4.1.1 *Experimental conditions.* Shearer *et al.* (1979) measured the radial profiles of the mean and rms velocity, and the Reynolds stress at three stations (z/D = 170, 340 and 510) for both isothermal single phase and vaporizing spray jet flows. For computational purposes, the profiles of turbulence dissipation rate (ϵ) at z/D = 170 is obtained from the shear stress measurements and the axial velocity gradient at the same station (z/D = 170). Also, the velocity distribution of the droplets (one group with an average diameter = 27 μm) is assumed to be the same as that of the carrier phase. This assumption will be discussed at the end of the next section. From the measurements of the droplets mass flux and velocity distribution, the volume fraction (Φ_2) is obtained. The profile of the Freon vapor concentration in the carrier phase (C) is obtained from the mixture fraction measurements and the state relations given by Shearer (1979). Table 1 summarizes all the starting profiles needed for the computation for both the single phase jet and the evaporating spray cases.

Temperature measurements of the carrier phase (with a bare wire chromelalumel thermocouple) showed only 5 °C difference either in the radial or the axial directions (between z/D = 170 and 510). On the other hand, Shearer's (1979) analysis showed that the droplet temperature at z/D = 170 is equal to the Feron's saturation temperature (240.3 K). In the present calculations we assumed that the temperature of the carrier phase is equal to the surrounding air temperature (296 K) and the droplets surface temperature is equal to the saturation one (240.3 K). At these conditions, the density of the liquid Freon-11 is equal to 1518 kg/m^3 and the vapor concentration at the droplets surface (C_L in [14] is equal to 0.292.

4.1.2 *Results and discussion.* Figure 1 shows the measured and predicted centerline decay of the mean axial velocity of the carrier phase compared to the single phase values. Due to the fact that the inertia of the droplets is much greater than that of the carrier phase (ρ_2/ρ_1 = 1520), the centerline velocities of the droplets are greater than those of the gas in the developing region. As a result, one would expect that the centerline velocity of the carrier phase to be greater than that of the single phase. This is due to (1) the continuous momentum transfer from the droplets to the gas since $V_{z,c}$ is greater than $U_{z,c}$, and (2) the reduction of the

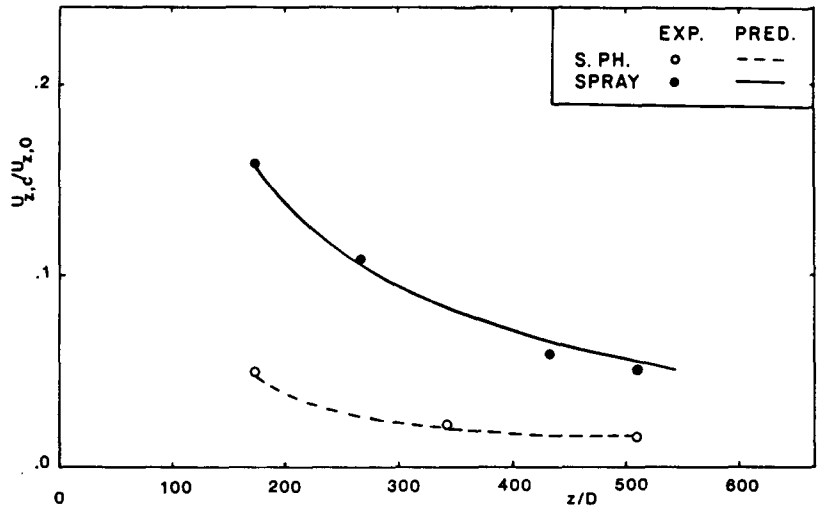

Figure 1. Axial variation of the centerline velocity (Freon-11 spray).

turbulence intensity (and hence turbulent diffusion) in the spray case compared to that of the single phase jet (as would be seen in figures 4 and 5).

Figures 2 and 3 show that normalized radial profiles of the mean axial velocities at 340 and 510 nozzle diameters from the exit plane for both the single phase jet and the evaporating spray cases. It can be seen from these figures that the jet width in the spray case is narrower than the single phase one. This result can be attributed to the increase of the centerline velocity of the carrier phase compared to its corresponding value in single phase jet. The experimental data show that with increasing the distance downstream from the nozzle exit, the jet behavior approaches that of the single phase figure 3). The effect of the droplets on the radial shear stress distribution is displayed in figures 4 and 5. It should be noted that the starting values of the turbulence quantities and mean velocity distribution of the vaporizing spray case differ (lower shear stress) from those of the single phase. This may have some effects on the profiles downstream ($z/D = 340$). In general, there is a reduction in the shear stress or an increase in the dissipation rate of the turbulence kinetic energy due to the presence of the liquid droplets in the same control volume with the carrier phase. As

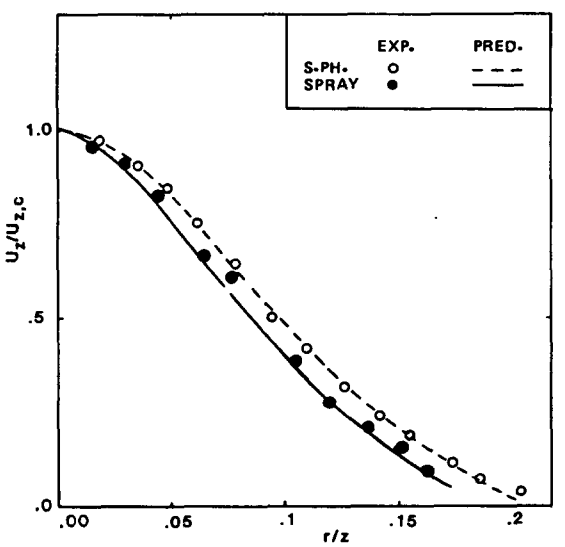

Figure 2. Radial variation of mean axial velocity at $z/D = 340$ (Feron-11 spray).

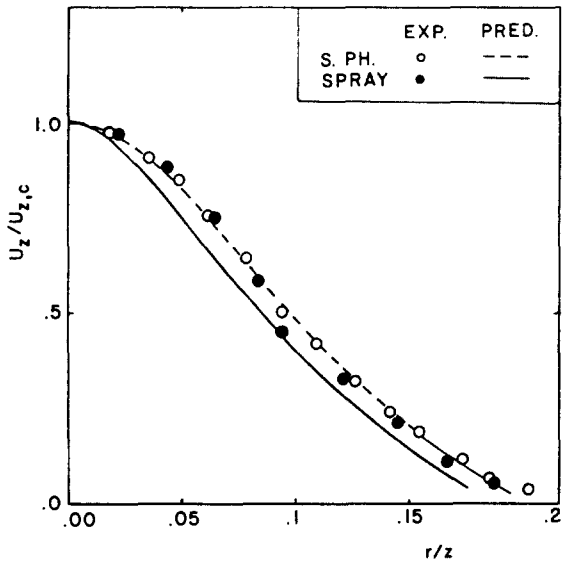

Figure 3. Radial variation of mean axial velocity at $z/D = 510$ (Feron-11 spray).

vaporization proceeds the effects of the droplets on the turbulence quantities diminish allowing the fluid behavior to approach that of a single-phase jet (figure 5).

In the present case we assumed that, at the starting station, the velocities of the droplets are equal to those of the gas. To study the effect of this assumption on the results, we increased the droplets velocity by 20%; the effect on the carrier phase profiles were negligible. This result can be attributed to two factors: (1) the droplets diameter, at the starting station, is equal to 27 μm, so the reduction rate of the mean relative velocity between the droplets and gas is considerable due to the vaporization. (2) Since the droplets mass fraction was measured, an increase in the velocity necessitates a reduction in the volume fraction. Thus the effects of increased velocity are counterbalanced by those of decreased volume fraction.

It is important to note that we neglected the effects of density fluctuation in the calculation. This assumption can be justified in this study since the mean density gradient is very small compared to the velocity gradient. This is due to the negligible evaporated mass compared to the entrained air, so the properties of the carrier phase are almost those of the standard air.

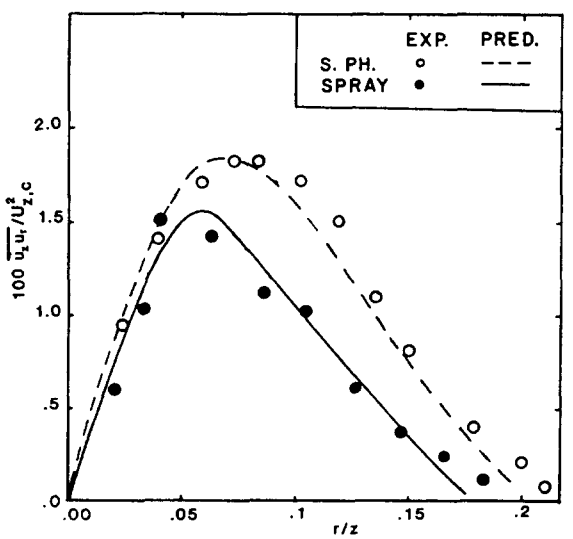

Figure 4. Radial variation of the shear stress at $z/D = 340$ (Freon-11 spray).

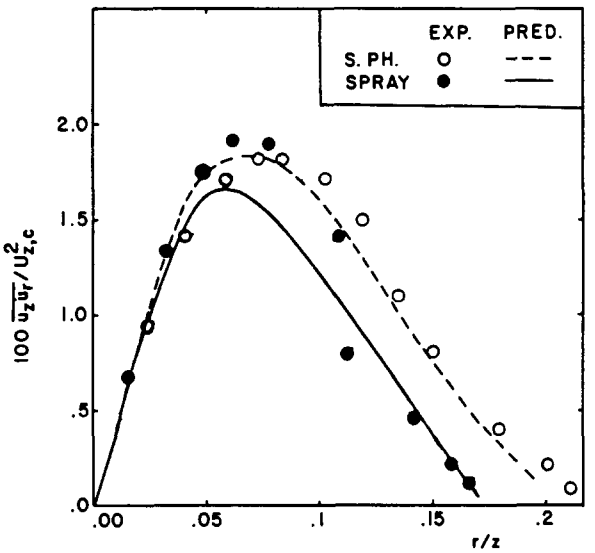

Figure 5. Radial variation of the shear stress at $z/D = 510$ (Feron-11 spray).

4.2 *The methanol spray*

The flow considered in this case is identical to that of Elghobashi *et al.* (1984) except that the solid spheres are replaced by liquid droplets of a given size distribution at the exit of the pipe. Our goal here is to mimic the flow of an idealized spray. The good agreement between our prediction and experimental data in the above section and in Elghobashi *et al.* (1984) allows us to use the same flow of the latter while adding the complexity of mass transfer and the resulting size changes in the same jet.

A turbulent round jet laden with multisize evaporating liquid droplets is considered in this work. Atmospheric air carrying methanol liquid droplets of diameters 100, 80, 60, 40 and 20μm issues vertically downwards from a cylindrical pipe of diameter D(=0.02 m). The velocity distributions are assumed to be fully developed at the pipe exit as in the work of Elghobashi *et al.* (1984). The ratio between the velocity of the dispersed phase to that of the carrier phase at the centerline is equal to 0.7. The carrier fluid Reynolds number is equal to 30,000 for all runs. The turbulence intensity distribution is taken as in the work of Elghobashi *et al.* (1984). The temperature of methanol droplets is assumed to be uniform at the steady state saturation conditions. The initial mass flow rates of the different size groups are assumed to be equal and have a plug profile for volume fractions. The ratio of the total mass flow rate of droplets to air (X_0) varies from 0.1 to 0.5.

4.2.1 *Results and discussion.* The normalized radial profiles of the mean axial velocities of the different phases at 20 pipe diameters from the exit plane and mass loading ratio $X_0 = 0.5$ are shown in figure 6. The mean velocities of the carrier phase and those of the five groups ($k = 1, 2, \ldots, 5$) of droplets are normalized by the centerline velocity of the single phase jet, $U_{c,s.ph.}$. Here $k = 1$ refers to the group that has the largest diameters, and $k = 5$ the smallest ones. It can be seen from this figure, as one would expect, that the velocity difference between the carrier phase and the largest diameter group is greater than that of any other group. This is attributed to the balance between the inertia of the droplet and the momentum exchange force. The inertia terms are proportional to $(d^k)^3$, whereas the momentum exchange force is proportional to the droplet diameter with an exponent ranging from 1 to 1.7 (for Reynolds number less than 100). Now dropping all the turbulent correlations in [1] with respect to the mean momentum exchange term, the equation becomes independent of Φ^k. By increasing the droplet size, the inertia becomes much greater than the momentum exchange forces, and as a result the relative velocity between the droplets and the carrier phase ($U_z - V_z^k$) increases. The volume fraction profile of each

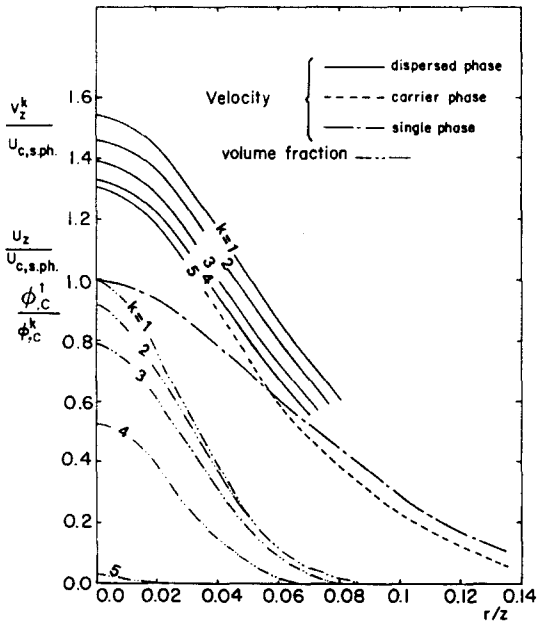

Figure 6. Normalized mean velocities and volume fractions profiles at $z/D = 20$ and at $X_0 = 0.5$ (methanol spray).

group normalized by the centerline value of the first group is shown also in figure 6. Since the reduction rate of the droplet diameter due to the evaporation process is inversely proportional to the square of the diameter (for small Reynolds number), the smaller the droplet diameter is the more reduction in the volume fraction. Figure 6 also shows that the smaller the mean droplet diameter is the less peaked (more diffusive) the volume fraction profile of its group. This is attributed to the turbulent diffusion coefficient (ν_p^k) of the droplet. This coefficient decreases with the increase of the droplet diameter [16]. In general, the radial diffusion of the droplet depends on the ratio of the droplet's relaxation time to the local Lagrangian integral time scale. It can be seen also from figure 6 that the mean velocity of the carrier phase is affected by the presence of the dispersed phase especially in the inner region. Elghobashi *et al.* (1984) discuss in detail how the entrainment and the negative radial velocity of the carrier phase in the jet outer region influence the volume fraction distribution of the dispersed phase. They showed that the entrainment creates an inward force exerted on the droplets towards the jet centerline. This force combined with the small turbulent diffusivity of the droplets, compared to that of the carrier phase, renders the volume fraction profile of the dispersed phase significantly narrower than the velocity profile of the carrier phase. Since the momentum exchange between the two phases is a linear function of the droplets volume fraction, one would expect that the momentum transfer to the carrier phase is maximum at the jet centerline. In the same time the reduction in the turbulence kinetic energy of the carrier phase and the increase of the dissipation rate of that energy due to the presence of the dispersed phase in the same control volume lead to a less turbulent diffusion coefficient for the carrier phase and hence a less radial diffusion of that phase compared to the single phase. These two factors make the velocity of the carrier phase at the jet centerline much greater than that of the single phase jet (30% higher) and less than its corresponding value in the jet outer region.

The influence of the loading ratio of the dispersed phase on the carrier fluid turbulence intensity and shear stress is displayed in figures 7 and 8. The reduction in the turbulence energy or the increase in the dissipation rate of that energy is caused by the fluctuating relative velocity between the droplets and the carrier phase and the turbulent correlation between this velocity and other fluctuating quantities (volume fractions and carrier fluid

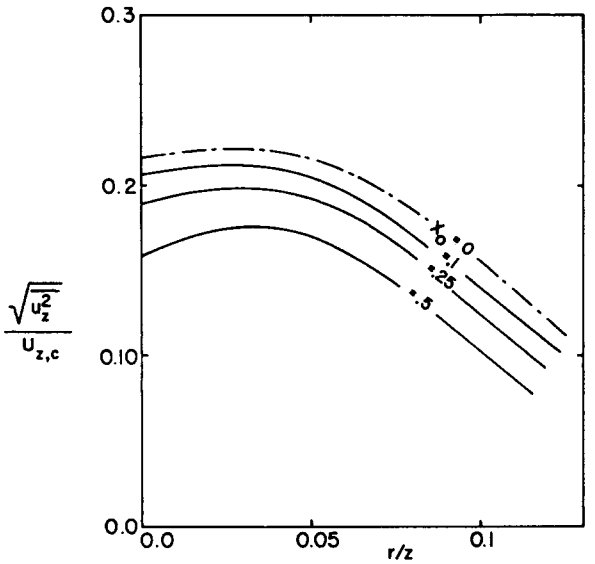

Figure 7. The turbulance intensity distribution under different mass loading ratios at z/D = 20 (methanol spray).

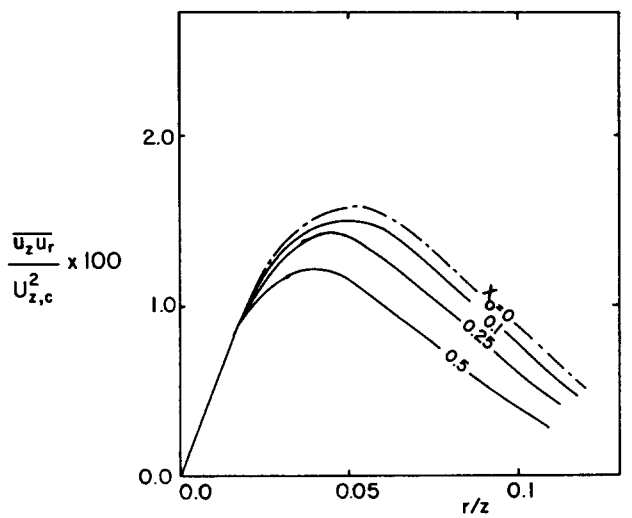

Figure 8. The shear stress distribution under different mass loading ratios at z/D = 20 (methanol spray).

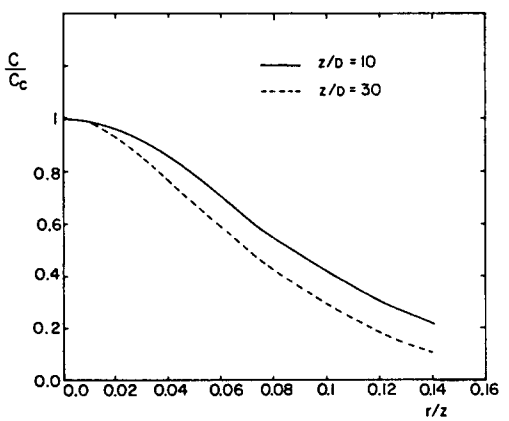

Figure 9. Normalized vapor concentration at different stations at X_0 = 0.5 (methanol spray).

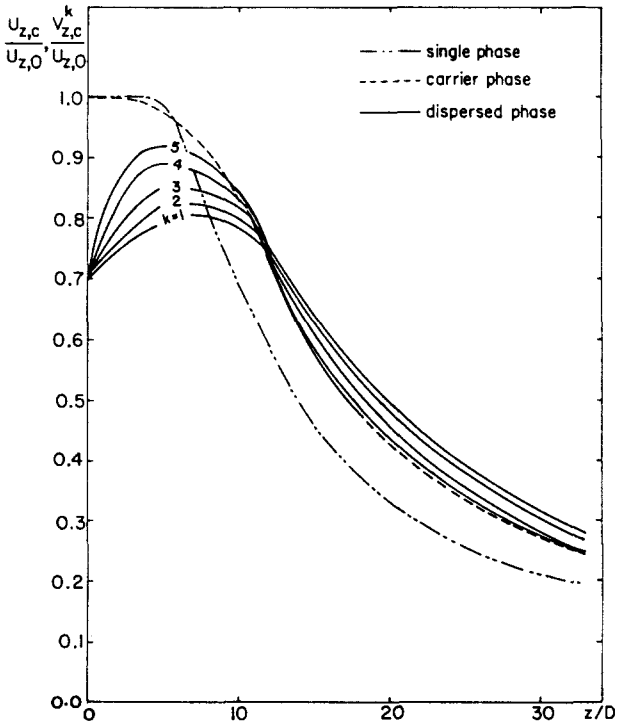

Figure 10. The axial distribution of the mean velocities at $X_0 = 0.5$ (methanol spray).

velocity). It can be stated that the reduction in the turbulence intensity and the shear stress is proportional to the mass loading ratio but not linearly.

The concentration of the evaporated material in the carrier phase is shown in figure 9 at two different axial locations ($z/D = 10$ and 30) and at $X_0 = 0.5$. Due to the continuous air entrainment by the jet and the turbulent diffusion of the vapor, the concentration of the evaporating material in the carrier fluid at $z/D = 30$ is less than the corresponding values at

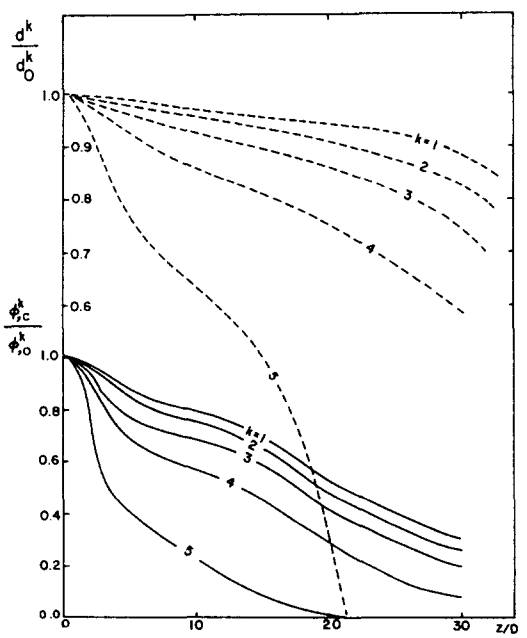

Figure 11. The axial distribution of the volume fractions and the average diameters at $X_0 = 0.5$ (methanol spray).

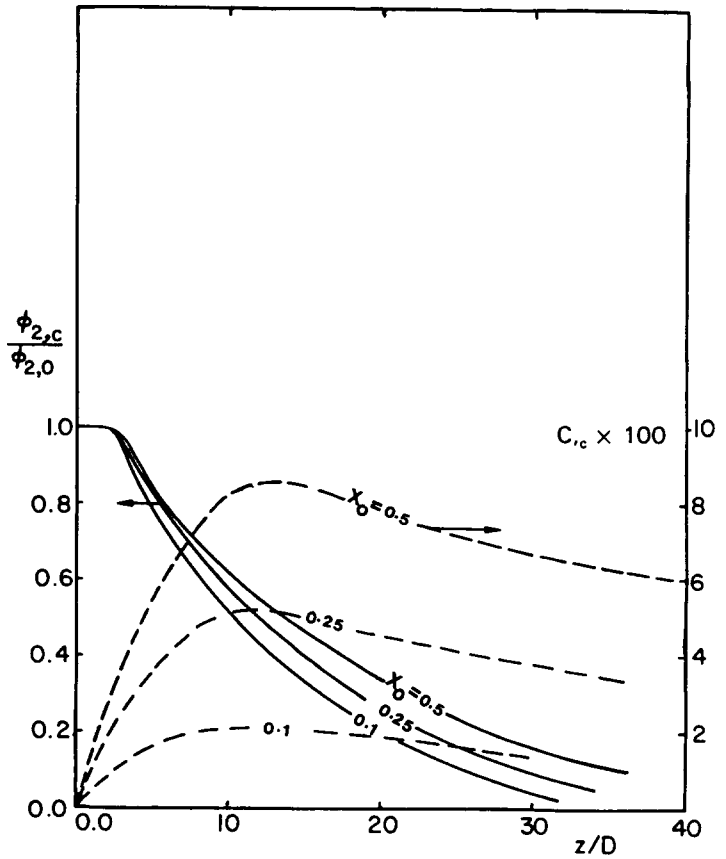

Figure 12. The axial distribution of the droplets volume fraction and vapor concentration (methanol spray).

$z/D = 10$ at the same distance from the jet axis, although the total evaporated mass increases with downstream distance. This is also true even at the jet centerline as will be seen in the discussion of figure 12.

It can be seen from figure 9 that C is minimum in the jet outer region and maximum at the jet centerline. Since C_L has a constant value of 0.12 calculated from [12] and [13], the transfer number [10] is maximum in the outer region of the jet. Therefore the diminution rate of the droplet diameter is greater in the outer than in the inner region.

Figure 10 shows that the centerline decay of the mean axial velocities of the different groups and the carrier phase compared to the single phase values for $X_0 = 0.5$. Here $U_{z,0}$ is the carrier-phase centerline velocity at the pipe exit. It can be seen that the relative velocity between the droplets and the carrier phase along the jet centerline increases with increasing the droplet diameter. It is worth noting that the carrier-phase centerline velocity ($U_{z,c}$) is about 30% higher than the corresponding value of the single phase in the range $7 \leq z/D \leq 30$ as discussed earlier.

Figure 11 exhibits the centerline decay of the volume fraction and mean droplet diameter based on the total surface area of the droplets for the five groups. The mean diameter is a quantity that is not used in the calculations but facilitates the display and discussion of the results. In the present work, we are able to calculate the local diameter distribution within each group, thus from the maximum and minimum diameters at any station and the number of sizes to be solved, the diameter range for each group can be fixed (e.g. at $z/D = 10$, group $k = 1$ contains droplets ranging from 95 to 78 μ). It can be seen from figure 6 that the smaller the droplet diameter is the higher the evaporation rate, hence the rapid decay of the volume fraction and the mean diameter.

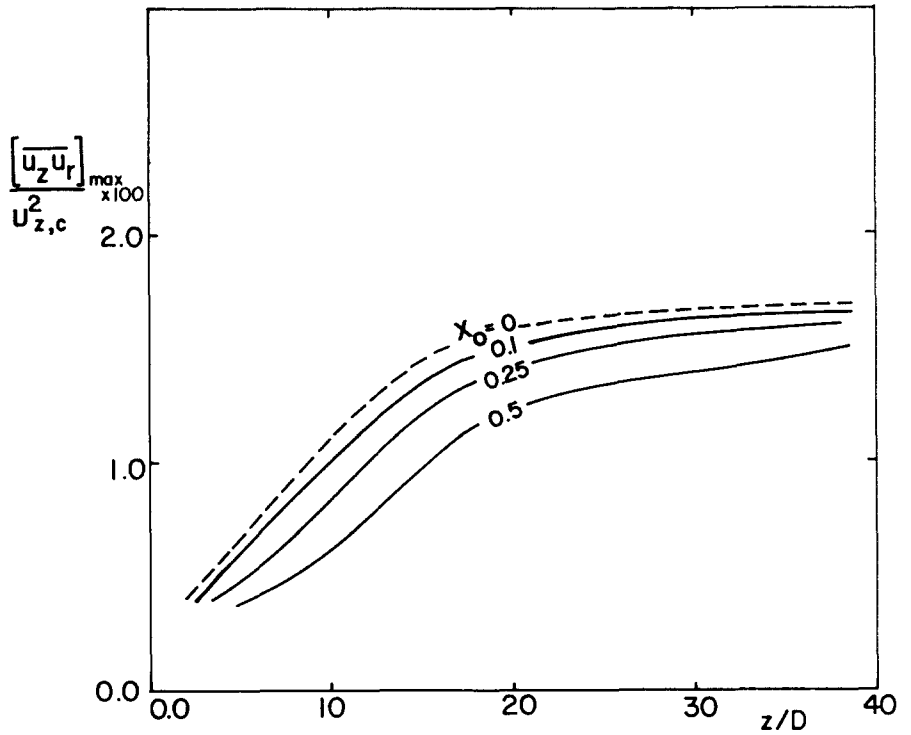

Figure 13. The axial distribution of the maximum turbulence intensity under different mass loading ratios (methanol spray).

Figure 12 shows the axial distribution of the total volume fraction of the droplets and the centerline concentration of the methanol vapor in the carrier phase (C_c) for different mass loading ratios. Here $\Phi_{2,c}/\Phi_{2,0}$ is the total volume fraction of the dispersed phase at the centerline divided by that value at the pipe exit. The concentration of the evaporated material in the carrier phase first increases until $z/D = 10$ then monotonically decreases due to the continuous air entrainment by the jet and turbulent diffusion of the vapor.

The variation of the maximum turbulence intensity and maximum shear stress of the carrier phase with the axial distance is displayed in figures 13 and 14 for different mass loading ratios. It can be seen that the reduction in the turbulence quantities is proportional to the mass loading ratio but again not linearly. Almost these two figures show that farther downstream from the pipe exit, the turbulence quantities are approaching their values for a single phase jet due to the continuous diminution of the droplets volume fraction.

The rate of evaporation is a function of both the transfer number and droplet Reynolds number which are maximum in the outer region and minimum at the centerline. So the rate of evaporation is maximum in the outer region, hence the minimum droplet diameter. This explains the radial distribution of the droplet diameter at the various sections as shown in figure 15. Also displayed is the monotonic reduction in droplet diameters with distance downstream for the five groups.

Figure 16 shows the effect of the evaporating spray on the spreading rate of the jet by comparing the different $Y_{1/2} \sim z$ distribution, where $Y_{1/2}$ is the radius at which the carrier-fluid mean axial velocity is half its value at the centerline. While for a turbulent single phase jet the value of the slope ($dY_{1/2}/dz$) is constant ($\simeq 0.08$), that for a two-phase jet is a function of the dispersed phase properties such as droplet diameter, density and mass loading ratio. This dependence was discussed in the work of Elghobashi *et al.* (1984). In the developing region the spreading rate of the spray case is much less than that for the single phase. As vaporization proceeds the effects of the droplets on the carrier fluid diminish allowing the fluid behavior to approach that of a single-phase jet.

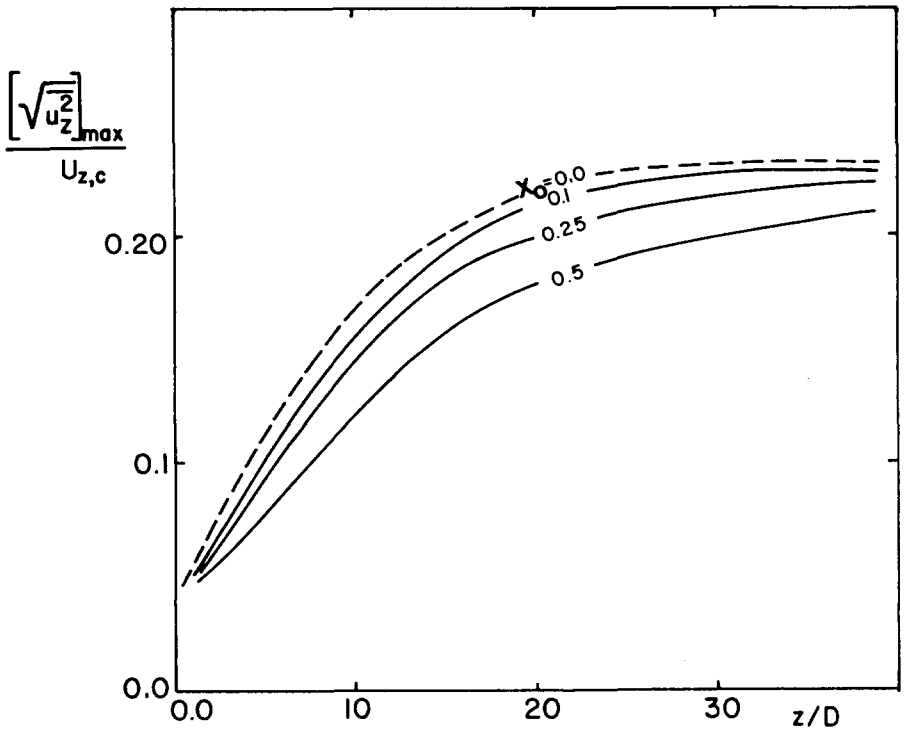

Figure 14. The axial distribution of the maximum shear stress under different mass loading ratios (methanol spray).

5. CONCLUDING REMARKS

A two-equation turbulence model for predicting two-phase jet flows with phase change is presented. The model is based on the exact transport equations of the turbulence kinetic energy and its dissipation rate derived from the two-phase momentum equations. The conversation equations of mass, momentum of each phase and concentration of vapor are solved to predict the flow of a turbulent jet laden with vaporizing droplets as a test for the mathematical model.

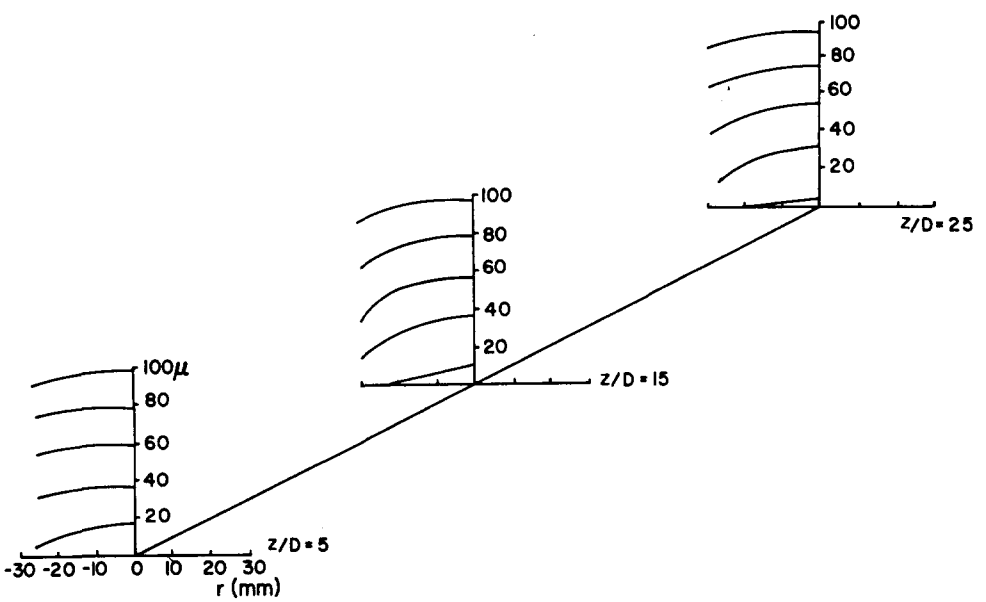

Figure 15. Radial distributions of the local droplets diameters at different axial locations and at X_0 = 0.5 (methanol spray).

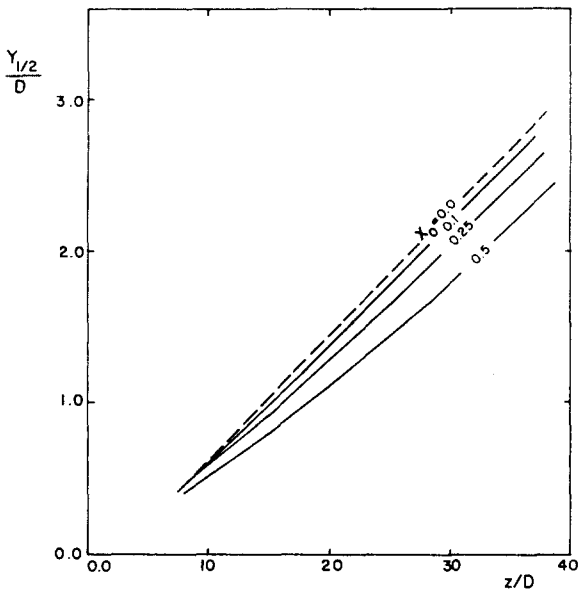

Figure 16. The spreading rate under different mass loading ratios (methonal spray).

The predictions show significant reductions in the turbulent shear stress and the kinetic energy of turbulence of the carrier phase due to the presence of droplets in the jet. This reduction is proportional to the mass loading ratio in a nonlinear manner.

The effect of the partial or complete droplet evaporation is reflected on the velocity distribution of the different groups. The smaller the droplet diameter is the less the relative velocity between the droplets and the fluid and the higher the turbulent diffusivity of that group. The radial distribution of the droplet diameters shows a continuous reduction accompanied by narrowing the radial extent of the dispersed phase. The jet spreading rate is significantly affected by the evaporation rate. Closer to the pipe exit the spreading rate is much less than that of the single phase jet. Farther downstream, it asymptotically approaches that of a single-phase jet.

In the region far away from the nozzle ($z/D \geq 170$), the predictions of Feron-11 spray are in a good agreement with the experimental data.

More validation testing of the model is needed via well-defined experiments.

Acknowledgements—This work has been supported by NASA-Lewis Research Center under Grant No. NAG-3-176. The authors express their thanks to Mrs. Verna Bruce for her expert typing of the manuscript.

REFERENCES

AL TAWEEL, A. M. & LANDAU, J. 1977 Turbulence Modulation in Two-Phase Jets. *Int. J. Multiphase Flow* **3**, 341–351.

ALONSO, C. V. 1981 Stochastic Models of Suspended Sediment Dispersion. *A.S.C.E.* **107**, 733–757.

CALABRESE, R. V. & MIDDLEMAN, S. 1979 The Dispersion of Discrete Particles in a Turbulent Fluid Field. *A.I.Ch.E.* **25**, 1025–1035.

CHAO, B. T. 1964 Turbulent Transport Behavior of Small Particles in Dilute Suspension. *Osterr, Ing. Arch.* **18**, 7–21.

CLIFT, R., GRACE, J. R. & WEBER, M. E. 1978 *Bubbles, Drops and Particles.* Academic Press, New York.

ELGHOBASHI, S. E. & ABOU-ARAB, T. W. 1983 A Two-Equation Turbulence Model for Two-Phase Flows. *Phys. Fluids* **25**, 931–938.

ELGHOBASHI, S., ABOU-ARAB, T., RIZK, M. & MOSTAFA, A. 1984 Prediction of the Particle-Laden Jet With a Two-Equation Turbulence Model. *Int. J. Multiphase Flow* **10**, 697–710.

HINZE, J. O. 1975 *Turbulence.* McGraw-Hill, New York.

LAUNDER, B. E., MORSE, A., RODI, W. & SPALDING, D. B. 1972 The Prediction of Free Shear Flows—A Comparison of the Performance of Six Turbulence Models. Imperial College, TM/TN/19.

INGEBO, R. D. 1956 Drag Coefficients for Droplets and Solid Spheres in Clouds Accelerating in Airstreams, NACA TN 3762.

MODARRESS, D., TAN, H. & ELGHOBASHI, S. 1984 Two-component LDA measurement in a two-phase turbulent jet. AIAA Journal **22**, 624–630.

MOSTAFA, A. A. & ELGHOBASHI, S. E. 1984 A Study of the Motion of Vaporizing Droplets in a Turbulent Flow. *Progr. Astronautics and Aeronautics*, **95**, 513–539. AIAA, New York.

MOSTAFA, A. A. 1985 A Two-Equation Turbulence Model for Dilute Vaporizing Sprays, Ph.D. Thesis, University of California, Irvine.

PESKIN, R. L. 1971 *Stochastic Estimation Applications to Turbulent Diffusion.* Int. Symp. Stochastic Diffusion (Edited by C.L. Chiu) University of Pittsburgh, Pittsburgh, Pa., 251.

RANZ, W. E. & MARSHALL, W. R. 1952 Evaporation from Drops. *Chem. Eng. Prog.* **48** (3), 141–146, 173–180.

SHEARER, A. J. 1979 Evaluation of a Locally Homogeneous Flow Model of Spray Evaporation Ph.D. Thesis, The Pennsylvania State University Park, Pa.

SHEARER, A. J., TAMURA, H. & FAETH, G. M. 1979 Evaluation of a Locally Homogeneous Flow Model of Spray Evaporation. *J. Energy* **3**, 271–278.

SHUEN, J. S., SOLOMON, A. S. P., ZHANG, Q. F. & FAETH, G. M. 1983 The Structure of Particle-Laden Jets and Nonevaporating Sprays. NASA CR 168059.

SOO, S. L. 1967 Fluid Dynamics of Multiphase Systems. Blaisdell, Waltham, Massachusetts, p. 59.

SPALDING, D. B. 1979 Numerical Computation of Multiphase Flows. Lecture notes, Thermal Sciences and Propulsion Center, Purdue University, West Lafayette, Ind.

WU, K.-J., Santavicca, D. A., BRACCO, F. V. & COGHE, A. 1984 LDV measurements of drop velocity in diesel-type sprays. AIAA Journal, **22**, 1263–1270.

YULE, A. J. SENG, C. AH, FELTON, P. G., UNGUT, A. & CHIGIER, N. A. 1982 A Study of Vaporizing Fuel Sprays by Laser Techniques. *Combustion and Flame* **44**, 71–84.